The magnetized sheath of a dusty plasma with nanosize dust grains

H. Mehdipour and G. Foroutan

Citation: Physics of Plasmas (1994-present) **17**, 083704 (2010); doi: 10.1063/1.3480099
View online: http://dx.doi.org/10.1063/1.3480099
View Table of Contents: http://scitation.aip.org/content/aip/journal/pop/17/8?ver=pdfcov
Published by the AIP Publishing

The magnetized sheath of a dusty plasma with nanosize dust grains

H. Mehdipour[1] and G. Foroutan[1,2]
[1]*Department of Physics, Faculty of Science, Sahand University of Technology, 51335-1996 Tabriz, Iran*
[2]*Nanostructure Material Research Center, Sahand University of Technology, 51335-1996 Tabriz, Iran and School of Physics, The University of Sydney, Sydney, New South Wales 2006, Australia*

(Received 20 April 2010; accepted 28 July 2010; published online 31 August 2010)

The magnetized sheath of a dusty plasma is investigated via numerical simulations of stationary multifluid equations by taking into account the electric, magnetic, gravitational, ion drag, neutral drag, and thermophoretic forces. Dependence of the sheath properties on the characteristics of the magnetic field and plasma parameters is explored. The sheath dynamics is mainly governed by the electric and ion drag forces and the effect of gravitation is negligible. The sheath demonstrates a nonmonotonic behavior against variations of the magnetic intensity and its angle of incidence. The sheath thickness and the maximum of dust density distribution decrease with increasing the ion to electron density ratio at the sheath edge, but increase with growing electron temperature and the positive temperature gradient of the neutrals. The effects of ion drag are similar to those of the gravitational force as both of them accelerate the dust to the wall. By a suitable configuration of the temperature gradient in the neutral gas, thermophoretic force can be utilized to deposit the building units of nanostructures on a substrate or remove any unwanted contaminant from its neighborhood. © *2010 American Institute of Physics*. [doi:10.1063/1.3480099]

I. INTRODUCTION

The investigation of plasma-wall transition is of great importance in different areas such as plasma-aided material processing, plasma probes, and plasma-assisted fabrication of ordered nanostructures.[1–3] Due to the different mobilities of electrons and ions the wall receives more electrons than ions and its potential remains negative with respect to the main body of plasma. This negative potential prevents further escape of the electrons toward the wall and leads to the separation of charges and formation of a sheath layer with a net positive charge near the wall. The scale of the sheath region is typically a few Debye lengths, while the quasineutrality scale is about the typical size of the system. To study the plasma and sheath structures, kinetic and hydrodynamic models are commonly employed. For a detailed consideration of using these models to describe the sheath region of a two component plasma, we refer to Refs. 4–12.

Dust particles are frequently encountered in laboratory plasmas such as processing discharges for etching, sputtering, and ion implantation.[1,13–18] The dust grains can be the impurity contaminants, introduced into the system by production tools or formed via agglomeration during the course of plasma processing. In plasma-assisted fabrication of microchips, particulate contaminant is a serious threat in the fabrication and must be removed from the processing environment, otherwise the unwanted contaminant compromises the performance and quality of the device. On the other hand, nanosize particles are introduced into plasma as building units for plasma-aided fabrication of different nanostructures. This is because, due to their large electric charge, site-selective and controlled deposition of nanoparticles is conceivable via the sheath electric field.[19–27]

The dynamics of dust particles in plasma sheath both in the presence and absence of an external magnetic field has been studied by several authors.[28–44] Ma and Yu[34] used a three-fluid model with Boltzmann distributed electrons and cold ion and dust fluids to describe the electrostatic sheath of a dusty plasma. They found that for small dust particles the sheath potential exhibits a solitonlike profiles and the dust density is strongly localized, while for larger dust grains a stratification of the dust density occurs. Davoudabadi and Mashayek[41] studied the sheath structure in the presence of an oblique magnetic field. In their one-dimensional model, the electrons are in thermal equilibrium, while the ions experience a friction force due to collisions with neutrals. They found that the sheath thickness decreases as the strength of the magnetic field increases and for low-pressures there exist optimums of the magnetic intensities for which the absolute charge on an isolated grain is minimum or maximum. Oscillations were observed in the spatial distribution of the ion velocity and density. Foroutan *et al.*[44] numerically investigated the structure of the magnetized sheath of a dusty plasma with micron size dust particles. Among the forces acting on the dust grains only the electrostatic, magnetic, and gravitational forces were taken into account. It was shown that above a threshold magnetic intensity, some kind of large regular inhomogeneities develops on the spatial profile of the dust particles. The sheath thickness shows nonlinear behavior against variations of the electron temperature and magnetic field intensity.

The present work is mainly motivated by the applicability of self-consistent sheath theory to plasma processing of materials and plasma-aided nanofabrication. The latter is a new and rapidly expanding multidisciplinary research area with continuously increasing importance both in fundamental research and technological applications.[3,24–27,45–54] Unlike conventional two component plasmas, dusty plasmas contain nanosize particles carrying dynamically variable charge, which can be used for deterministic and controlled synthesis

of a broad range of nanomaterials and nanoassemblies.[27] The navigation of the flux of nanoparticles for their site-specific deposition is made possible via the electric field of the plasma sheath. This task is facilitated by the inhomogeneous electric field of a prepatterned nanostructure array on the substrate. Due to their large electric charge, the role of dust particle in determination of the sheath potential cannot be neglected at high dust densities and a self-consistent description of plasma sheath should include their contribution in the space charge. Our literature review shows that the dynamics of a magnetized dusty plasma sheath, with dust as a fluid, has not been investigated in the presence of drag and thermophoretic forces, while these forces are crucial in controlling and management of the plasma particle fluxes impinging on the substrate. Moreover, due to the collection of plasma particles by dust grains, the dust acts as sinks for electrons and ions and in a self-consistent description their effects should be included in the continuity equations.

In this paper, we investigate the impacts of plasma parameters and the characteristics of an externally applied oblique magnetic field on the structure of a dusty plasma sheath. To simulate the real situation, a self-consistent three-fluid model including the effects of electric, magnetic, thermophoretic, ion drag, neutral drag, and gravitational forces on the dust grains is employed. The space charge of dust particles is included in the Poisson equation for the sheath potential. The loss of the electrons and ions to the dust, collisions of the plasma particles with neutrals, and the electron impact ionization of neutrals are taken into account in the corresponding fluid equations. The orbit motion limited (OML) theory is used to calculate the charge of the dust particles. The set of fluid equations, Poisson equation, and equations for dust charging are solved numerically to obtain the spatial distribution of the sheath quantities. The effects of variations in the strength and angle of incidence of the magnetic field, as well as the plasma parameters at the sheath edge on the ion, electron, and dust normal speeds, their densities, dust charge, and the electrostatic sheath potential are explored and the implications for plasma-aided nanofabrication are discussed.

This article is organized as follows. In Sec. II the multifluid sheath model is introduced, the main assumptions are given, and the numerical procedure is outlined. The results of numerical simulations for the sheath structure and particle distributions are presented and discussed in Sec. III. The article is concluded with a summary of the main findings and an outlook for future work in Sec. IV.

II. NUMERICAL MODEL AND BASIC EQUATIONS

Figure 1 shows a schematic description of the sheath configuration used in this study. The plasma-sheath boundary is located at $z=0$, where the electrostatic potential is zero, with plasma filling the region $z<0$. It is assumed that the sheath is homogenous in x and y directions and the variations of the physical parameters are considered in z direction. The magnetic field is constant in space and time and lies in the (x,z) plane making an angle with the z axis.

The conventional fluid approach is employed to investigate the dynamics of the plasma particles and the structure of the sheath. Although there exists a temperature gradient in the neutral gas, the neutrals are assumed motionless. However, the electrons and ions are treated as fluids with constant temperatures throughout the sheath. The set of governing equations are the continuities

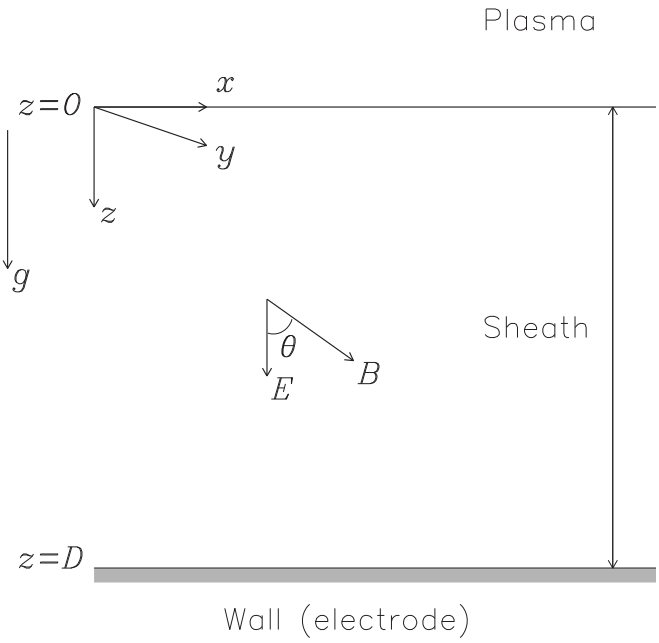

FIG. 1. The geometry of the magnetized plasma sheath.

$$\frac{d}{dz}(n_d v_{dz}) = 0, \tag{1}$$

$$\frac{d}{dz}(n_i v_{iz}) = \gamma_{\text{ion}} n_n n_e - \nu_{id} n_d, \tag{2}$$

$$\frac{d}{dz}(n_e v_{ez}) = \gamma_{\text{ion}} n_n n_e - \nu_{ed} n_d \tag{3}$$

and momentum equations

$$m_d v_{dz} \frac{dv_{dx}}{dz} = \frac{q_d}{c} B v_{dy} \cos\theta + F_{idx} + F_{ndx}, \tag{4}$$

$$m_d v_{dz} \frac{dv_{dy}}{dz} = \frac{q_d}{c} B(v_{dz} \sin\theta - v_{dx} \cos\theta) + F_{idy} + F_{ndy}, \tag{5}$$

$$m_d v_{dz} \frac{dv_{dz}}{dz} = -q_d\left(\frac{d\phi}{dz} + \frac{B}{c} v_{dy} \sin\theta\right) + m_d g + F_{idz} + F_{ndz} + F_{thz}, \tag{6}$$

$$m_i v_{iz} \frac{dv_{ix}}{dz} = \frac{e}{c} B v_{iy} \cos\theta - m_i \nu_{in} v_{ix}, \tag{7}$$

$$m_i v_{iz} \frac{dv_{iy}}{dz} = \frac{e}{c} B(v_{iz} \sin\theta - v_{ix} \cos\theta) - m_i \nu_{in} v_{iy}, \tag{8}$$

$$m_i v_{iz}\frac{dv_{iz}}{dz} = -e\left(\frac{d\phi}{dz} + \frac{B}{c}v_{iy}\sin\theta\right) - \frac{T_i}{n_i}\frac{dn_i}{dz} - m_i\nu_{in}v_{iz}, \tag{9}$$

$$0 = -\frac{e}{c}Bv_{ey}\cos\theta - m_e\nu_{en}v_{ex}, \tag{10}$$

$$0 = -\frac{e}{c}B(v_{ez}\sin\theta - v_{ex}\cos\theta) - m_e\nu_{en}v_{ey}, \tag{11}$$

$$0 = e\left(\frac{d\phi}{dz} + \frac{B}{c}v_{ey}\sin\theta\right) - \frac{T_e}{n_e}\frac{dn_e}{dz} - m_e\nu_{en}v_{ez} \tag{12}$$

for the dust grains, ions, and electrons, respectively. In the above equations, m_j is the mass, n_j is the number density, v_{jx}, v_{jy}, and v_{jz} are the x, y, and z components of the fluid velocities of particle species j, and ϕ and q_d are the electric potential and charge of the dust grains, respectively. ν_{jn}, and ν_{jd} are, respectively, the collision frequency with neutrals and the loss frequency of plasma particle species j due to attachment to the dust. The loss frequency is proportional to the corresponding particle current onto the dust grain, $\nu_{jd}=|I_j|/e$. The electrostatic potential is obtained from the Poisson equation

$$\frac{d^2\phi}{dz^2} = 4\pi e(n_e - n_i - z_d n_d), \tag{13}$$

where z_d is the charge number of the dust grain. The quasineutrality condition at the sheath edge is

$$e(n_{i0} - n_{e0}) + q_{d0}n_{d0} = 0. \tag{14}$$

The ionization rate γ_{ion} depends on the ionization potential of the neutrals and for the argon plasma considered here is given by[1]

$$\gamma_{\text{ion}} = 5\times 10^{-8}\exp\left(-\frac{15.8}{T_e}\right). \tag{15}$$

In the above equations the electron inertia and ion-electron and electron-dust collisions have been neglected. The ion drag $\boldsymbol{F}_{id}$ consists of a collection component and an orbit component given by[55]

$$\boldsymbol{F}_{id}^{\text{coll}} = \pi r_d^2 n_i m_i V_{it}\bar{\boldsymbol{v}}_{\boldsymbol{i}}\left(1 - \frac{2eq_d}{r_d m_i V_{it}^2}\right), \tag{16}$$

$$\boldsymbol{F}_{id}^{\text{orb}} = 2\pi b_0^2 n_i m_i V_{it}\bar{\boldsymbol{v}}_i \ln\left(\frac{b_0^2 + \lambda_{De}^2}{b_0^2 + b_c^2}\right), \tag{17}$$

where r_d is the dust radius, $V_{it}=(\bar{v}_i^2 + 8T_i/\pi m_i)^{1/2}$ is the total ion speed, $\bar{\boldsymbol{v}}_i$ is the directed ion speed relative to a dust particle moving with velocity v_d, $b_0=eq_d/(m_i v_i^2)$ is the impact radius corresponding to a 90° deflection, and $b_c=r_d(1-2b_0/r_d)^{1/2}$ is the direct collision impact parameter. The neutral drag force $\boldsymbol{F}_{dn}$ is given by the Epstein expression

$$\boldsymbol{F}_{nd} = -\tfrac{8}{3}\sqrt{2\pi}r_d^2 m_n n_n v_{Tn}\boldsymbol{v}_d, \tag{18}$$

where $v_d \ll v_{Tn}$ and v_{Tn} is the neutral thermal speed defined as $v_{Tn}=\sqrt{T_n/m_n}$. Finally, the thermophoretic force on the dust grain, amid a neutral gas with a temperature gradient $\nabla_z T_n$, is approximated by

$$\boldsymbol{F}_{th} \approx -\frac{5}{4\sqrt{2}}\left(\frac{r_d}{\sigma_{LJ}}\right)^2\nabla_z T_n, \tag{19}$$

where σ_{LJ} is the Lennard-Jones collision diameter of the gas. The OML expressions for the local plasma currents I_j, $j=i,e$, flowing onto the grains are

$$I_j = \pi r_d^2 n_j q_j V_{jt}\left(1 - \frac{2q_j q_d}{r_d m_j V_{jt}^2}\right) \tag{20}$$

for $q_j q_d < 0$ (attractive potential) and

$$I_j = \pi r_d^2 n_j q_j V_{jt}\exp\left(-\frac{2q_j q_d}{r_d m_j V_{jt}^2}\right) \tag{21}$$

for $q_j q_d > 0$ (repulsive potential), where subscript j represents plasma particle species j. As the ions in the sheath have a directed speed toward the wall, the ion thermal velocity, $v_{Ti}=\sqrt{T_i/m_i}$, has been replaced with ion mean speed V_{it}. But the directed electron speed is very small compared to its mean thermal speed, then for the total electron speed we have $V_{et}\approx\sqrt{8T_e/\pi m_e}$. The magnetic field intensities, for which OML theory can be utilized are limited to $B<B_{cr}$, where B_{cr} is given by

$$B_{cr}(\text{kG}) = \frac{41.37}{r_d(\mu\text{m})}\sqrt{\frac{T_e(\text{eV})}{3(\text{eV})}}. \tag{22}$$

This condition corresponds to $r_d<\rho_e$, where $\rho_e=\sqrt{T_e m_e c^2/e^2B^2}$ is the electron gyroradius. In calculation of dust charge, the local plasma currents are considered. This is because the time required for a grain to be charged from zero to floating potential is much smaller than of the dust motion. Thus, the charging process can be regarded as a local phenomenon and the equilibrium grain charge is obtained from

$$I_e + I_i = 0. \tag{23}$$

To describe the dust dynamics using continuous fluid model, the intergrain distance, $d=n_d^{-3}$, should be smaller than the electron Debye length. Moreover, the OML theory requires d to be larger than the ion Debye length λ_{Di}. Therefore, with $n_{i0}\approx n_{e0}=10^{12}$ cm^{-3}, $T_e=1$ eV, and $T_i=0.05$ eV, the present study is applicable for dust densities $1.9\times10^9 < n_d < 3.6\times10^{11}$ (in cm^{-3}). In this range the effects of drag forces and loss of plasma particles to dust grains are noticeable and should be taken into account.

To obtain the numerical solutions, we rewrite Eqs. (1)–(15) in dimensionless form using the following set of normalized variables:

$$N_j = n_j/n_{j0}, \quad \boldsymbol{u}_{i,e} = \boldsymbol{v}_{i,e}/c_{si}, \quad \boldsymbol{u_d} = \boldsymbol{v}_d/c_{sd},$$

$$\bar{\nu}_{in} = \nu_{in}/\omega_{pi}, \quad \bar{\nu}_{en} = m_e\nu_{en}/m_i\omega_{pi}, \quad \bar{\nu}_{\text{ion}} = \nu_{\text{ion}}/\omega_{pi}, \tag{24}$$

$$\bar{\nu}_{jd} = \nu_{jd}/\omega_{pi}, \quad \Phi = e\phi/T_e, \quad \xi = z/\lambda_{De}, \quad Q_d = eq_d/r_d T_e.$$

Here $c_{si}=\sqrt{T_e/m_i}$, and $c_{sd}=\sqrt{ZT_e/m_d}$ are, respectively, the ion-acoustic and dust acoustic speeds and the parameter $Z=r_d T_e/e^2$ is dust charge number when its surface potential

is T_e/e. $\nu_{\text{ion}}=n_n\gamma_{\text{ion}}$ and $\omega_{pi}=\sqrt{4\pi n_{i0}e^2/m_i}$ are, respectively, the ionization and ion plasma frequencies. $\lambda_{De}=\sqrt{T_e/4\pi n_{e0}e^2}$ is the electron Debye length and Q_d is the normalized dust charge.

Using the above normalized variables, Eqs. (1)–(15) can be written in dimensionless form as follows

$$\frac{dN_d}{d\xi}=Q_d\frac{N_d}{u_{dz}^2}\left(\frac{d\Phi}{d\xi}+\delta\beta_d u_{dy}\sin\theta\right)-\mu\frac{N_d}{u_{dz}^2}(m_d g+F_{idz}+F_{ndz}+F_{thz}), \tag{25}$$

$$\frac{du_{dx}}{d\xi}=Q_d\delta\beta_d\frac{u_{dy}}{u_{dz}}\cos\theta+\frac{\mu}{u_{dz}}(F_{idx}+F_{ndx}), \tag{26}$$

$$\frac{du_{dy}}{d\xi}=Q_d\delta\beta_d\left(\sin\theta-\frac{u_{dx}}{u_{dz}}\cos\theta\right)+\frac{\mu}{u_{dz}}(F_{idy}+F_{ndy}), \tag{27}$$

$$\frac{du_{dz}}{d\xi}=-\frac{Q_d}{u_{dz}}\left(\frac{d\Phi}{d\xi}+\delta\beta_d u_{dy}\sin\theta\right)+\frac{\mu}{u_{dz}}(m_d g+F_{idz}+F_{ndz}+F_{thz}), \tag{28}$$

$$\frac{dN_i}{d\xi}=-\frac{N_iT_e}{T_i-u_{iz}^2T_e}\left(\frac{d\Phi}{d\xi}+\delta\beta_i u_{iy}\sin\theta+\delta\bar{\nu}_{in}u_{iz}\right)-\frac{\delta^{-1}T_e u_{iz}}{T_i-u_{iz}^2T_e}\left[N_e\bar{\nu}_{\text{ion}}-\frac{(1-\delta^2)}{ZQ_{d0}}N_d\bar{\nu}_{id}\right], \tag{29}$$

$$\frac{du_{ix}}{d\xi}=\frac{\delta}{u_{iz}}(\beta_i u_{iy}\cos\theta-\bar{\nu}_{in}u_{ix}), \tag{30}$$

$$\frac{du_{iy}}{d\xi}=\frac{\delta}{u_{iz}}[\beta_i(u_{iz}\sin\theta-u_{ix}\cos\theta)-\bar{\nu}_{in}u_{iy}], \tag{31}$$

$$\frac{du_{iz}}{d\xi}=-\frac{1}{u_{iz}}\left(1-\frac{T_i}{T_i-u_{iz}^2T_e}\right)\times\left(\frac{d\Phi}{d\xi}+\delta\beta_i u_{iy}\sin\theta+\delta\bar{\nu}_{in}u_{iz}\right)+\left[\bar{\nu}_{\text{ion}}N_e-\frac{(1-\delta^2)}{ZQ_{d0}}\bar{\nu}_{id}N_d\right]\frac{\delta^{-1}T_i}{N_i(T_i-u_{iz}^2T_e)}, \tag{32}$$

$$\frac{dN_e}{d\xi}=N_e\frac{d\Phi}{d\xi}-N_e\delta\bar{\nu}_{en}u_{ez}\left[1+\frac{\sin^2\theta}{\cos^2\theta+(m_i\bar{\nu}_{en}/m_e\beta_e)^2}\right], \tag{33}$$

$$\frac{du_{ez}}{d\xi}=-u_{ez}\frac{d\Phi}{d\xi}+\delta\bar{\nu}_{en}u_{ez}^2\left[1+\frac{\sin^2\theta}{\cos^2\theta+(m_i\bar{\nu}_{en}/m_e\beta_e)^2}\right]+\frac{\delta}{N_e}\left(\bar{\nu}_{\text{ion}}N_e-\frac{(1-\delta^2)}{ZQ_{d0}}\bar{\nu}_{ed}N_d\right), \tag{34}$$

$$\frac{d^2\Phi}{d\xi^2}=N_e-\delta^2N_i-(1-\delta^2)N_d\frac{Q_d}{Q_{d0}}, \tag{35}$$

where $\delta=(n_{i0}/n_{e0})^{1/2}$, $\mu=\lambda_{De}/(m_d c_{sd}^2)$, $\beta_d=(Zm_i/m_d)^{1/2}\beta_i$, and $\beta_{i,e}=\omega_{ci,e}/\omega_{pi}$. The cyclotron frequency is given by $\omega_{cj}=|e|B/m_jc$ with $j=i,e$. The parameters $\beta_{i,e}$ and ν_{jn}, respectively, measure the importance of the magnetic force and the collisional momentum exchange in the plasma momentum equations. For numerical integration of the above equations we employ the following boundary conditions at the sheath edge ($\xi=0$):

$$u_{ex,y,z}=u_{ix,y}=u_{dx,y}=0,\quad u_{iz}=1,\quad u_{dz}=5,\qquad N_{d,i,e}=1,\quad \Phi=0,\quad \frac{d\Phi}{d\xi}=\bar{\nu}_{in}. \tag{36}$$

As we are interested in applicability of self-consistent sheath theory to plasma-aided nanofabrication, a large dust Mach number is assumed at the sheath edge. This value is necessary for the nanoparticles to overcome the repelling electric force, which prevents them from reaching the substrate. Otherwise, the dust particles are suspended between the substrate and the sheath edge. Actually, negatively charged nanoparticles can obtain large momentum when they pass through wide presheath areas.[56,57] Experimental and numerical results show that nanosize particles can move with the same speed as that of ions which is much larger than the dust acoustic speed.[58]

The set of Eqs. (25)–(35) with boundary conditions (36) are solved using a fourth-order-Rung–Kutta method, while the Eq. (23) is simultaneously solved to obtain the dust charge in the magnetized plasma sheath.

III. NUMERICAL RESULTS AND DISCUSSION

This section presents the results of numerical simulations for the sheath structure and spatial distributions of the density and velocity of the plasma particles in an oblique magnetic field. We consider an argon plasma with constant ion and electron temperatures: $T_i=0.05$ eV and $T_e=1$ eV. Other default parameters are $n_{e0}=10^{12}$ cm^{-3}, $n_n=10^{15}$ cm^{-3}, $\delta^2=1.5$, $\bar{\nu}_{in}=0.01$, $\bar{\nu}_{en}=0.002$, $\nabla_z T_n=-55$ K cm^{-1}, $r_d=40$ nm, and $\rho_d=2.0$ g cm^{-3}, where ρ_d is the mass density of the grains. The magnetic field intensity and the angle of incidence are, respectively, $B=35$ kG and $\theta=45°$, the former is in the range of laboratory generated magnetic strengths. The position of the wall or electrode is determined from the value of its potential, considered to be $\Phi_w=-15$ in the present work.

First we compare the magnitudes of different forces acting on the dust particles. Figure 2 shows the spatial distributions of the electric F_E, magnetic F_B, ion drag F_{id}, neutral drag F_{nd}, gravitational F_g, and thermophoretic F_{th}, forces for different values of the electron temperature and electron number density. It is clearly seen that, for the set of default parameters chosen in this paper, the dynamics of the nanoparticles is mainly governed by the electric and ion drag forces. The latter always accelerates the dust toward the wall, but the former decelerates them almost throughout the sheath

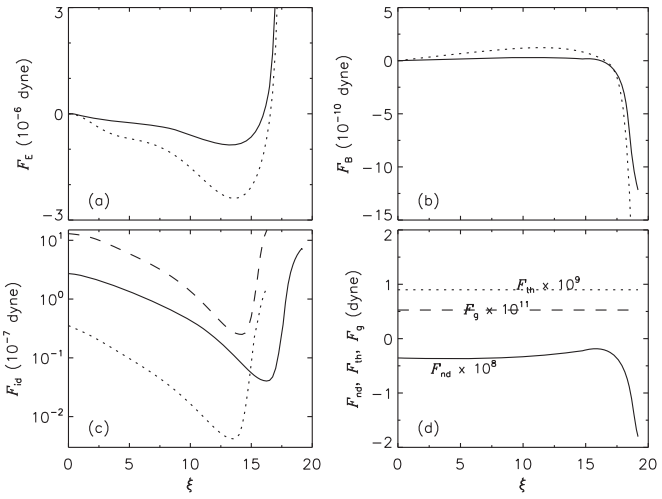

FIG. 2. The spatial profiles of the main forces acting on the nanoparticles: (a) the electric force F_E and (b) magnetic force F_B, solid and dotted curves are for $T_e=1$ eV and $T_e=2$ eV, respectively; (c) the ion drag force F_{id}, for $n_{e0}=10^{11}$ cm^{-3} (dotted) and $n_{e0}=10^{12}$ cm^{-3} (solid) with $r_d=40$ nm, and for $n_{e0}=10^{12}$ cm^{-3} with $r_d=100$ nm (dashed); (d) the neutral drag F_{nd} (solid), gravitational F_g (dashed), and thermophoretic forces of a negative temperature gradient F_{th} (dotted) all as functions of ξ.

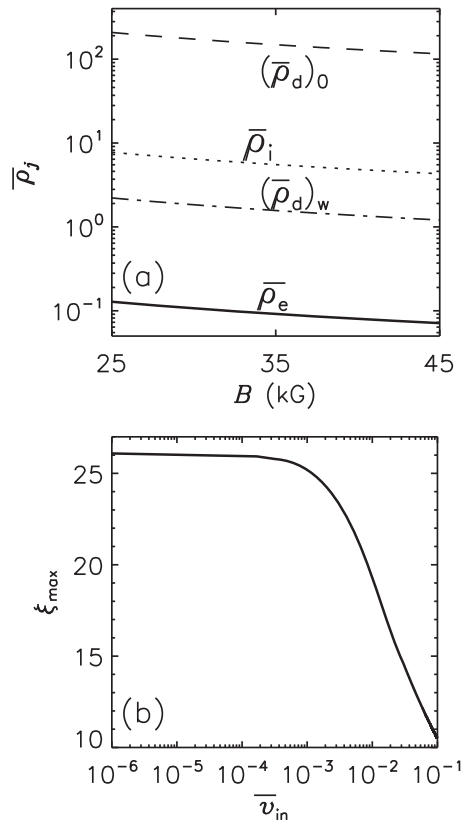

FIG. 3. (a) The dependence of the normalized gyroradius $\bar{\rho}_j$ of species j on the magnetic intensity with $\bar{\rho}_e$ (solid) for electrons, $\bar{\rho}_i$ (dotted) for ions, $(\bar{\rho})_0$ (dashed) for dust at the sheath edge, and $(\bar{\rho})_W$ (dotted-dashed) for dust close to the wall. (b) The dependence of sheath width $\xi_{\max}$ on the normalized ion-neutral frequency $\bar{\nu}_{in}$.

except for near the substrate where the dust pass through the charge reversal point. The charge reversal point is a point along the sheath where the negatively charged nanoparticles change sign and become positive. Along the sheath, the absolute electric force increases, while ion drag decreases such that somewhere before the charge reversal point they balance each other and the dust density shows its maximum. The magnitudes of both electric and ion drag forces increase with increasing the absolute dust charge and consequently with the electron temperature, electron number density, and the dust radius which is obvious from Figs. 2(a) and 2(c). The neutral drag force, directed away from the wall, is at least an order of magnitude smaller than the ion drag but its effect is appreciable near the wall where the magnetic force is also large. Gravitational force is almost negligible in this study but thermophoretic force can play a role in the sheath dynamics especially if the neutral temperature gradient sets to large values by external means.

To identify the physical regime of the system and degrees of magnetization and collisionality, Fig. 3 demonstrates the normalized gyroradius $\bar{\rho}_j=\rho_j/\lambda_{De}$ of species j as a function of the magnetic intensity for electrons, ions, and dust particles (both near the sheath edge and close to the wall). Dependence of the sheath width on the normalized ion-neutral frequency has also been plotted. To calculate the dust gyroradius it is assumed that the dust particles have the same temperature as the ions. If $\bar{\rho}_j$ is less than or of the order of unity then the corresponding species j is magnetized. But if $\bar{\rho}_j \gg 1$ then the species j is weakly magnetized. It is understood from Fig. 3(a) that for default magnetic field intensity $B=35$ kG the electrons, the dust particles near the wall and probably the ions can be treated as magnetized. But the dust particles near the edge are weakly magnetized. Variations of the sheath width with $\bar{\nu}_{in}$ in Fig. 3(b) indicate that for $\bar{\nu}_{in}<0.001$, the sheath width is independent of the collision frequency. But for higher values of $\bar{\nu}_{in}$ it decreases with increasing of the collision frequency. For our default value of $\bar{\nu}_{in}=0.01$ the sheath may be considered collisional.

Figure 4 shows the spatial distributions of the dust charge, the dust normal speed, and the dust and plasma particle densities as functions of ξ for three different values of the magnetic field intensity and two different angles of incidence. The sheath shows a nonmonotonic dependence on the angle of incidence; the sheath thickness decreases with increasing the magnetic strength at moderate angles of incidence but increases with B at large values of θ (magnetic field almost parallel to the wall). Our numerical results showed that u_{iy} and u_{dy} are positive across the sheath. Therefore, according to Eqs. (28), (32), and (34), the magnetic force enhances the z component of the velocity of electrons and negatively charged grains and reduces that of the ions. But when the dust charge changes sign and becomes positive, the magnetic force reverses its direction and as a result the normal speed of the dust decreases, as is obvious from Fig. 2(b). Since the magnetic force is much smaller than the electric and drag forces, it affects the dust distribution almost indirectly via the variations of the electrons and ions distributions. The strength of the magnetic force increases with increasing θ. The net positive charge across the sheath increases when θ varies from small to moderate values. So, a narrower sheath is needed to provide the Debye shielding. But then at much larger values of θ, due to accumulation of

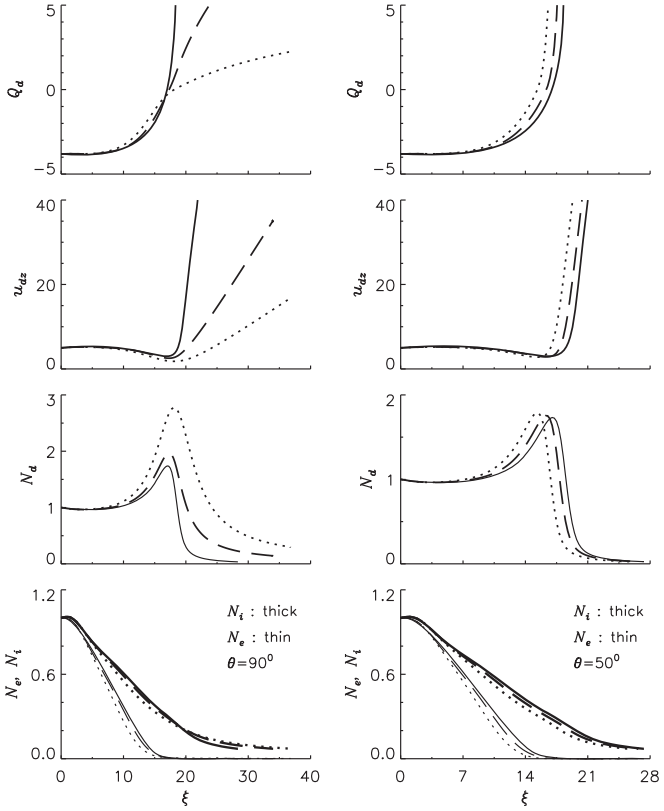

FIG. 4. The effects of variation of the magnetic field intensity on the dust charge, the particle densities, and the dust normal speed for three different values of the magnetic field intensity with θ=90° (left column) and θ=50° (right column). The solid, dashed, and dotted curves correspond to B=5, 27, and 45 kG, respectively. Here, Φ_w=−100 and all other parameters are set to their default values.

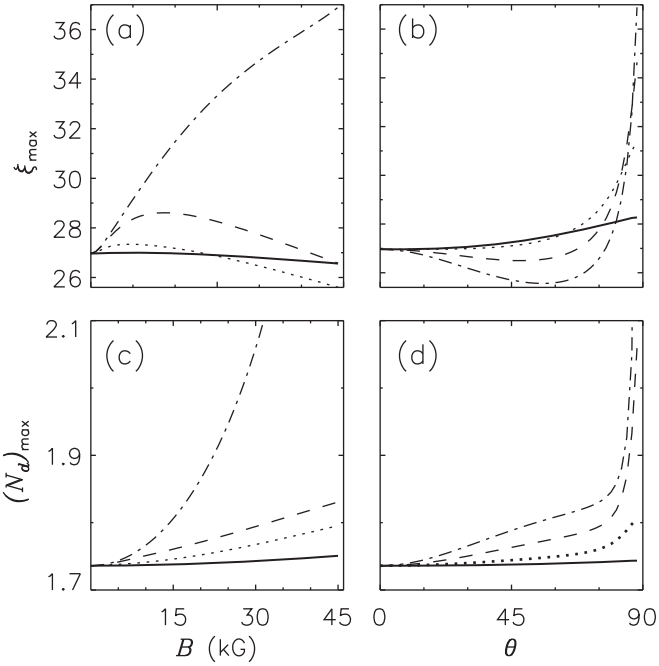

FIG. 5. Dependence of the sheath width ξ_{max} and peak of the dust number density $(N_d)_{max}$ on the magnetic field intensity and its angle of incidence. (a) solid, dotted, dashed, and dotted-dashed curves are for θ=20°, θ=50°, θ=75°, and θ=88°, respectively. (b) ξ_{max} as a function of θ, B=5 kG (solid), 15 kG (dotted), 30 kG (dashed), and 45 kG (dotted-dashed). (c) $(N_d)_{max}$ as a function of B for the same angles of incidence as in (a). (d) $(N_d)_{max}$ as a function of θ for the same magnetic intensities as in (b).

dust particles near the wall, which is obvious from dotted N_d curve in Fig. 4, the net positive space charge decreases and the sheath is broadened. This point can also be inferred from dotted Q_d curve which declines for large ξ. We find from Q_d curves in the left column that at large angles of incidence the charge reversal point moves away from the wall as the magnetic field intensity increases. It should be noted that the position of the wall is not the same for the three cases.

Figure 5 shows the dependence of the sheath thickness ξ_{max} and the peak of dust number density $(N_d)_{max}$ on the magnetic strength and its angle of incidence. It is seen that at small angles of incidence (solid curve) the sheath thickness decreases with increasing the magnetic field intensity. As the angle of incidence increases, ξ_{max} first increases with B but then at higher values of B it decreases. For magnetic fields almost parallel to the wall, the sheath width always increases with the magnetic intensity. Figure 5(b) shows that for a given magnetic field intensity the sheath thickness decreases with increasing the angle of incidence up to a specific value and then increases rapidly for lager values of θ. Therefore, as mentioned above, the sheath thickness demonstrates a nonmonotonic dependence on the magnetic field intensity and its angle of incidence. We find from Figs. 5(c) and 5(d) that the peak of the dust number density is an increasing function of B and θ. Inspection of N_d curves in Fig. 4 reveals that the width of the dust layer demonstrates a similar behavior. The dust distribution is determined by the spatial profiles of the dust relevant forces which depend directly or indirectly on the spatial distributions of the electrons and ions. These distributions, in turn, are affected by the presence of the dust and the external magnetic field. Therefore, dusty plasma sheath is a self-organized structure[36] which adjusts itself in such a way that the suspended dust particles grow both in the number density and spatial width with increasing the effect of the magnetic field.

As the charge of a dust particle depends strongly on its radius, the latter plays an important role in the formation and structure of the sheath. To investigate the effects of dust radius on the sheath quantities, Fig. 6 displays the spatial distribution of the dust charge, the electrostatic potential, and the normal speeds and number densities of the dust and plasma particles for three different dust radii. It is seen that the sheath thickness and the densities of electrons, ions, and dust particles decrease while the normal speeds of ions and dust increase. To explain this effect, we note that according to Eqs. (20) and (21) the plasma current flowing onto the dust particles is proportional to the square of the dust radius. Therefore, more plasma particles are collected by the larger dust and consequently the corresponding plasma particle densities decrease. As more electrons attach to dust particles than ions, the positive charge density increases with increasing the dust radius, leading to a narrower plasma sheath. Moreover, for larger grains the gravitational and ion drag forces dominate over other forces and accelerate the dust to the wall. So the dust normal speed increases and consequently its density decreases. Higher kinetic energy gains for

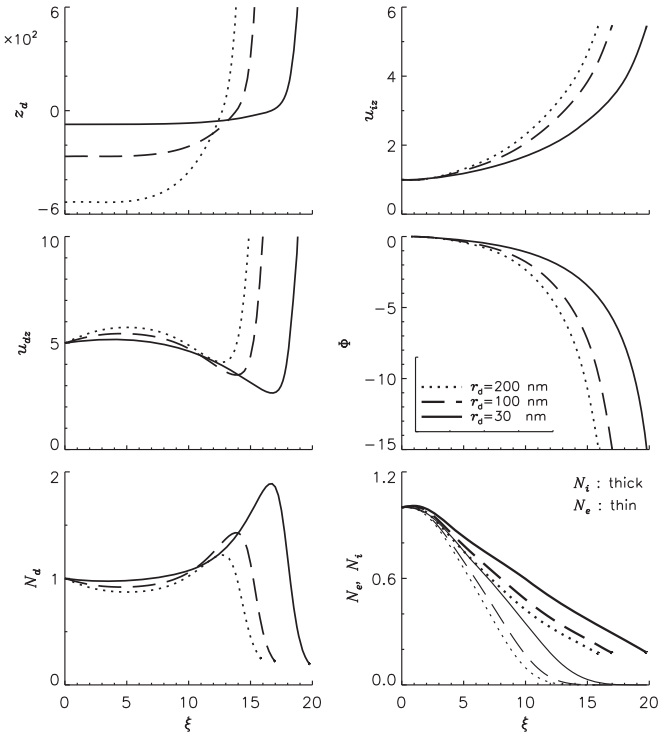

FIG. 6. The effects of variation of dust radius on the dust charge, the sheath potential, the particle densities, and the particle normal speeds.

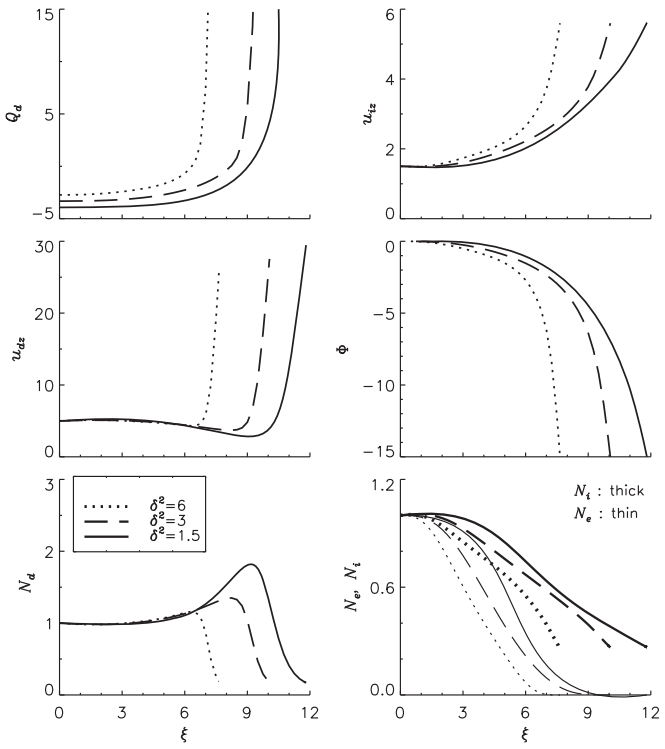

FIG. 7. The distributions of the dust charge, the sheath potential, the particle densities, and the particle normal speeds as functions of ξ for three different values of the ratio of ion-to-electron density at the sheath edge. Here the ion Mach number is M_i=1.5 and all the other parameters are set to their default values.

larger grains are evidenced by the microgravity experiments reported by Fortov *et al.*[59] From the above discussion it is clear that the dust radius is a key parameter in transport and deposition of nanoparticles on a substrate. It can be used to manage the flux and kinetic energy of the incident grains. It should also be noted that the increase of the absolute dust charge (the surface potential of the dust grain) with increasing of the dust size has been observed experimentally.[60] This is also obvious from z_d-curves in Fig. 6.

In experimental setups the dust are introduced to the environment via an ultrasonic vibrator attached to a dust reservoir and the dust density is dependent on the voltage of the sinusoidal signal applied to the vibrator.[18] So, the dust density can be easily adjusted to a specific value via changing the voltage. Furthermore, in a dusty plasma the ratio of the ion to electron number density is larger than unity and increasing of this ratio is equivalent to increasing of the dust number density, provided that the dust radius remains unchanged. Figure 7 shows the effect of variation of the dust number density on the sheath structure and particles distributions. The sheath thickness decreases with increasing the ratio of ion-to-electron number density at the edge. This is because for larger dust number densities, more plasma particles attach to the grains and as a result both the ion and electron densities are reduced, but the reduction is more efficient for electrons than ions. Therefore, the net positive charge density increases in the sheath and a narrower sheath can protect the plasma against the wall potential. It is seen that the absolute dust charge decreases with increasing the dust number density and changes sign quickly close to the wall. The changes in the sheath thickness and absolute dust charge are consistent with experimental results of Adhikary *et al.*[18] Dependence of the sheath width on the dust radius and the ratio of the ion to electron density at the sheath edge is presented in Fig. 8. The sheath thickness decreases with increasing of the dust radius and/or the dust number density.

It is known experimentally that the ion drag is an important factor in dynamics of nanosize grains and its effect cannot be neglected at large plasma densities.[61] To investigate the effect of ion drag force on the sheath structure and spatial distribution of the particles, we have plotted in Fig. 9 the sheath quantities both in the presence and absence of the ion drag force. The effects of ion drag on the dust are similar to those of gravitational force, as both of them accelerate the dust toward the wall. Therefore, the dust number density decreases efficiently near the wall and as a result the net positive charge density increases inside the sheath which in turn leads to a narrower plasma sheath.

Now we study the effects of variation of the bulk plasma parameters on the structure of the sheath. Figure 10 displays the structure of the sheath for three different values of the ion Mach number. We see that the ion Mach number has strong influence on the sheath structure and particle distributions. The sheath thickness and the dust number density decrease with increasing ion Mach number. This is due to the fact that, for fast ions, the decelerating collisional and magnetic forces are less effective and the ions flow easily toward the wall and become more populated than the electrons so the sheath width decreases. It is seen from the dashed and dotted Q_d curves that for larger ion Mach numbers the dust charge changes sign quickly and becomes positive as we move away

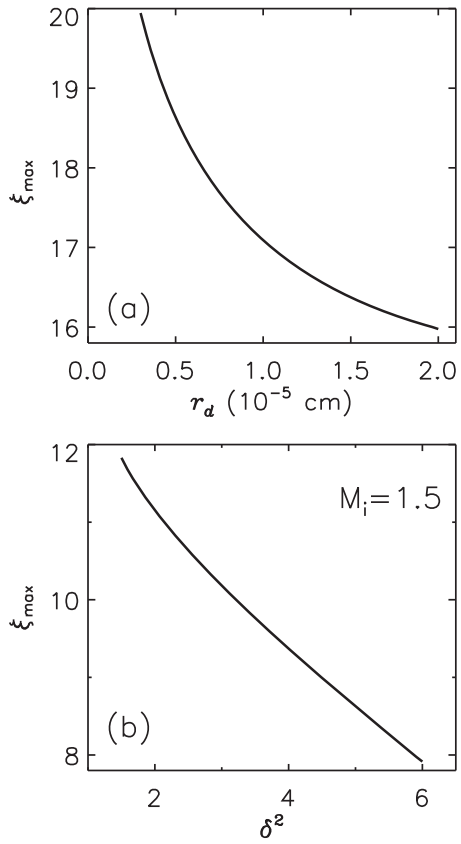

FIG. 8. Dependence of the sheath width ξ_{max}: (a) on the dust radius r_d and (b) the ratio of ion-to-electron density at the sheath edge δ^2.

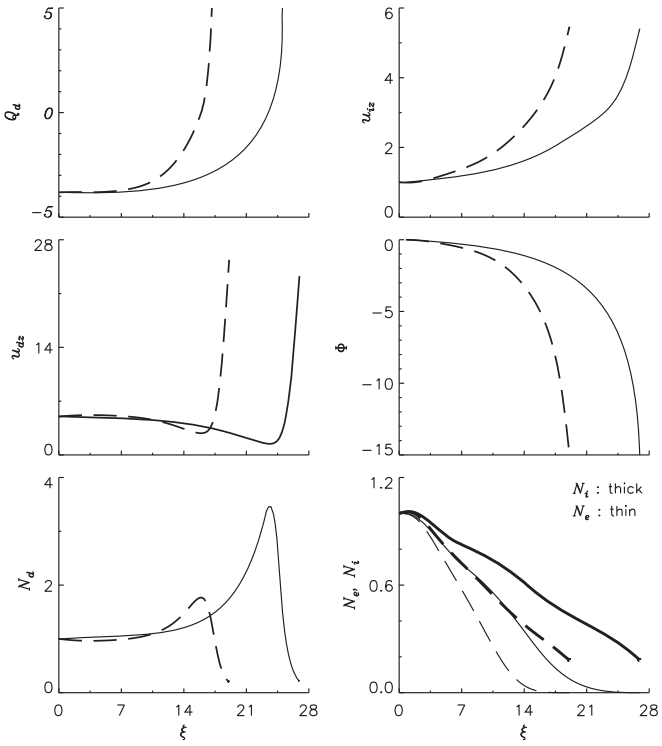

FIG. 9. The effects of the ion drag force on the sheath structure. The dashed curves are in the presence of the ion drag force and solid curves are when the ion drag force is switched off.

from the sheath edge. This is of special importance for plasma-aided nanofabrication, as positively charged nanoparticles can be strongly influenced by the horizontal electric fields of a prefabricated pattern (e.g., an array of conducting nanotips) on a substrate and become focused on the nanostructures.

Experimental and computational results show that thermophoretic force plays an important role in the plasma-assisted fabrication of different nanostructures.[57] From Eq. (19), it is seen that thermophoretic force is proportional to the neutral temperature gradient and can be away or toward the substrate. This provides an efficient means of managing and controlling the flux of nanosize dust grains for nanofabrication. By a suitable choice of the experimental conditions, thermophoretic force can be used to deposit the building units on the nanostructures or remove unwanted contaminants from the substrate. Figure 11 represents the effects of neutral temperature gradient on the sheath structure and spatial distributions of the particles. Applying a positive temperature gradient, i.e., when the neutral gas temperature increases as we approach the wall, leads to enhancement of the sheath width and the density of dust particles. The dust and ion speeds decrease near the wall, but the ion density increases. To understand this behavior, it is noted that the thermophoretic force is in opposite direction to the temperature gradient. A positive temperature gradient creates a thermophoretic force directed toward the sheath edge. Then the nanoparticles are slowed down and their density increases close to the wall. The net positive charge of the sheath decreases and as a result the sheath is broadened. Due to accumulation of dust particles near the wall, the spatial profile of the electric field changes such that the ion normal speed decreases close to the wall and its number density increases. From the solid curves in Fig. 11 we find that the negative temperature gradient has inverse effects. Since different temperature gradient configurations can be easily reached by external heating of the substrate, the thermophoretic force is an important means of controlling the transport and deposition of nanoparticles on a substrate or removing unwanted contaminants away from the surface.

Figure 12 displays variations of the dimensional sheath width z_{max} and the peak of the dust distribution $(N_d)_{max}$ with the electron temperature T_e and the neutral temperature gradient ∇T_n. We find that the sheath is broadened and the peak dust density grows with increasing T_e and ∇T_n. To explain the expansion of the sheath with T_e, it is noted that the electron distribution can be fairly approximated by the Boltzmann relation, $n_e = n_{e0} \exp(e\phi/T_e)$. Increasing the electron temperature leads to the enhancement of the electron number density.[62,63] As a result, more electrons are collected by the dust grains and the absolute dust charge increases. Then, the magnetic and electric forces on the dust become stronger and decelerate them more effectively, leading to enhancement of the dust number density near the wall. Consequently, the net positive charge decreases and the sheath is broadened. The dependence of $(N_d)_{max}$ on ∇T_n is very interesting. Above a specific temperature gradient (approximately 50 K cm^{-1}) the peak dust density grows up quickly with increasing the temperature gradient. These temperature gradients can easily be

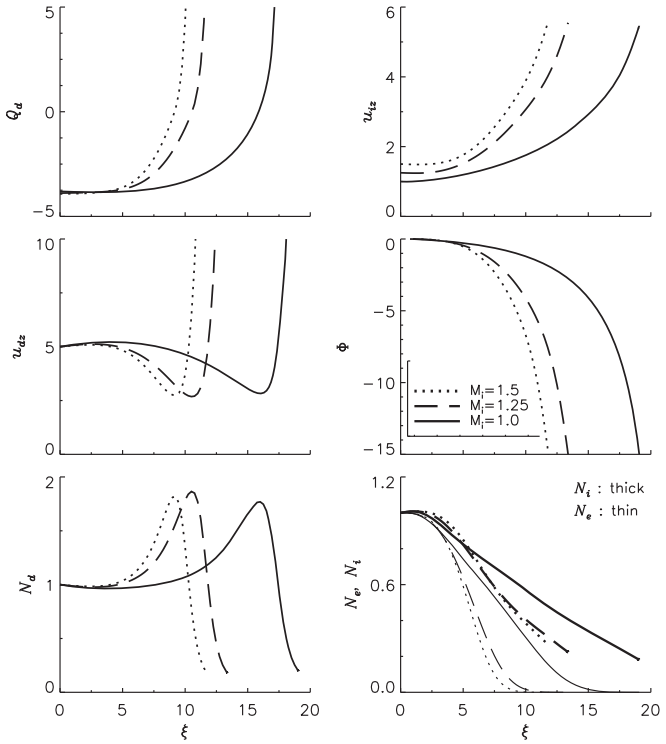

FIG. 10. Profiles of the dust charge, the sheath potential, the particle densities, and the particle normal speeds as functions of ξ for three different ion Mach numbers.

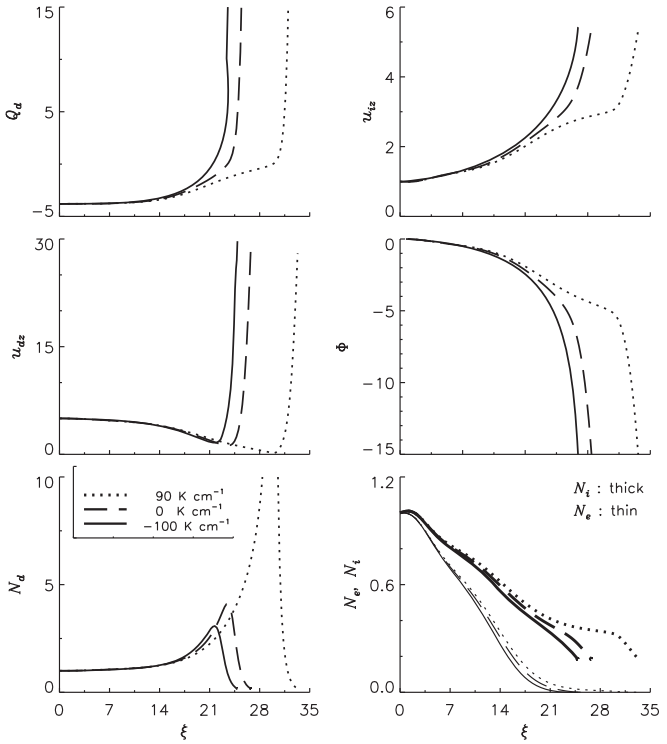

FIG. 11. The results of the numerical simulations for distribution of the normalized dust charge, the sheath potential, the particle densities, and the particle normal speeds for three different values of the neutral temperature gradient. Here $n_{e0}=10^{10}$ cm^{-3} and all the other parameters are set to their default values.

reached in laboratory plasma setups by externally driven heating devices.[57]

IV. SUMMARY AND CONCLUSIONS

Using numerical simulations of three-fluid sheath model, we investigated the dynamics and structure of a dusty plasma sheath in the presence of an oblique magnetic field, by taking into account the electric, magnetic, gravitational, drag, and thermophoretic forces. We studied the effects of the plasma and magnetic field parameters on the formation and properties of the sheath and examined the applicability of the results for plasma nanofabrication. The main findings are summarized as follows:

- The electric and ion drag forces are the most important forces which control the dynamics of the nanoparticles. These forces balance each other at a point along the sheath where maximum in the dust density distribution occurs. The gravitational force is not important in the present work for the dust particles suitable for plasma nanofabrication. The magnetic force on the dust particles becomes appreciable only close to the wall, but it is believed that it affects the dust particles throughout the sheath via changing the electrons and ion density distributions and as a result the charging of the dust.
- The sheath demonstrates a nonmonotonic behavior against variations of the magnetic field intensity and its angle of incidence. At small angles of incidence the sheath width decreases with increasing θ, while the reverse is happening at large angles. Likewise, for a given magnetic field intensity, the sheath thickness decreases with increasing θ from small to moderate values, but then it is broadened with further increasing of θ to large values. Other sheath parameters such as the normal speeds and densities of the ions and nanoparticles are strongly affected by variations of the magnetic field parameters. Since different magnetic field configurations can be easily reached through applying an external setup, then this provides us with an efficient means of controlling and manipulating the deposition flux on a substrate.
- Changing the dust radius affects the sheath structure in different ways. First, we note that a dust particle is like a spherical capacitor and its charge is proportional to its radius. Therefore, more plasma particles attach to the larger dust and for a given dust number density this leads to enhancement of the net positive charge inside the sheath and hence the reduction of the sheath thickness. Second, it is obvious from Eqs. (16)–(19) that the drags and thermophoretic forces are proportional to the square of the dust radius while the proportionality of the gravitational force is cubic. Therefore, at large dust radii the gravitation dominates the other forces and accelerates the dust to the wall leading to reduction of the dust number density near the wall. Since the ion drag is in the same direction as the gravitation, while the neutral drag in the opposite direction, the ion drag strengthens the effects of gravitational force but the neutral drag weakens them.
- Thermophoretic force can be easily invoked to deposit the building units of nanostructures or remove any unwanted contaminant from the vicinity of the substrate. Positive

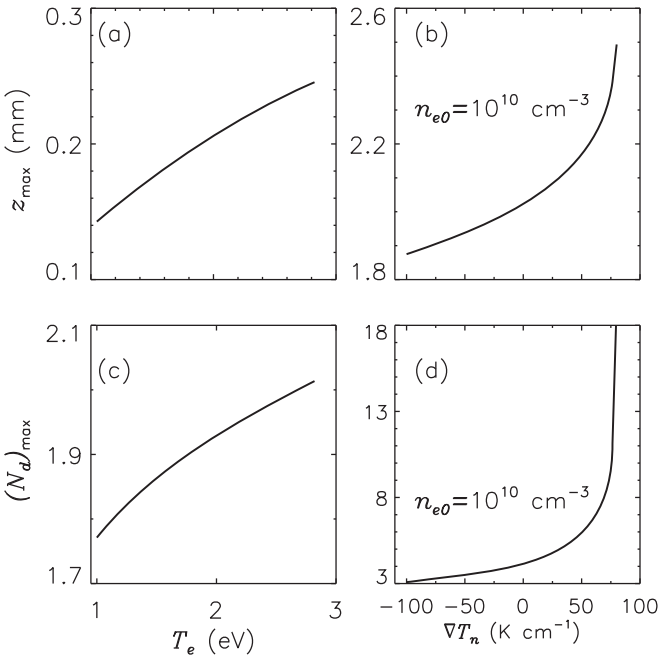

FIG. 12. Variations of the dimensional sheath width z_{max} and peak of the dust distribution $(N_d)_{max}$ with: (a) and (c) the electron temperature T_e and (b) and (d) the neutral temperature gradient ∇T_n.

temperature gradients prevent nanoparticles from reaching the wall while negative gradients accelerate them. In the case of positive temperature gradients the sheath is broadened and the peak of dust number density increases near the wall but the reverse is true for negative gradients. It should be mentioned here that the surface kinetic requirements for the formation and growth of different structures with different composition may restrict the range of applicable temperature gradients.

- The sheath width and the maximum of the dust number density distribution decrease with increasing the ion to electron density ratio at the sheath edge, but increase with growing electron temperature and positive temperature gradient of neutrals. It seems that they are correlated in some way.
- Dusty plasma sheath is a self-organized structure, i.e., changing any parameter of the plasma particles or the external magnetic field affects the whole sheath quantities such as the sheath width, its potential, and the velocities and distributions of the particles.
- The stratification of the dust spatial profile and other sheath parameters found in our previous work,[44] for micron size dust grains, is not observable in the present work. This can be attributed to small dust grains and large dust Mach numbers considered here.
- The suspension of dust particles inside the plasma sheath (dust with zero velocity) has been frequently observed in the experiments. But for the plasma and dust parameters chosen in this work (aimed at exploring the applicability of the sheath theory to plasma nanofabrication) most of the dust grains can reach the charge reversal point and then are accelerated by the electric force toward the wall. Therefore, in the present study we are not concerned about the suspension or reflection of the dust particles. But in different situations where the suspension or reflection of dust particles is a concern one should use different approaches such as Lagrangian particle equations to describe these phenomena.

The results presented here are quite general and can be utilized in a wide range of applications including plasma processing of materials, plasma-aided fabrication of different nanostructures and thin films, and coatings. In this work we neglected the effect of any horizontal electric field or inhomogeneities produced by a growing structure on the substrate. Future work will incorporate such considerations to simulate the real situation in the plasma nanofabrication.

ACKNOWLEDGMENTS

This work was supported by Sahand University of Technology.

[1] M. A. Lieberman and A. J. Lichtenberg, *Principle of Plasma Discharges and Material Processing* (Wiley, New York, 1994).
[2] I. H. Hutchinson, *Principles of Plasma Diagnostics*, 2nd ed. (Cambridge University Press, Cambridge, 2002).
[3] K. Ostrikov and S. Xu, *Plasma-Aided Nanofabrication from Plasma Source to Nanoassembly* (Wiley, Weinheim, 2007).
[4] V. A. Godyak and N. Sternberg, IEEE Trans. Plasma Sci. **18**, 159 (1990).
[5] K.-U. Riemann, J. Phys. D **24**, 493 (1991).
[6] X. P. Chen, Phys. Plasmas **5**, 804 (1998).
[7] R. N. Franklin, J. Phys. D **36**, R390 (2003).
[8] K.-U. Riemann, J. Phys. D **36**, 2811 (2003).
[9] K.-U. Riemann, Phys. Plasmas **13**, 063508 (2006).
[10] T. E. Sheridan and J. Goree, Phys. Fluid B **3**, 2796 (1991).
[11] H.-B. Valentini, Phys. Plasmas **3**, 1459 (1996).
[12] B. Alterkop, J. Appl. Phys. **95**, 1650 (2004).
[13] J. E. Daugherty and D. B. Graves, J. Appl. Phys. **78**, 2279 (1995).
[14] M. Takai, T. Nishimoto, M. Kondo, and A. Matsuda, Appl. Phys. Lett. **77**, 2828 (2000).
[15] A. A. Samarian, B. W. James, S. V. Vladimirov, and N. F. Cramer, Phys. Rev. E **64**, 025402 (2001).
[16] A. A. Samarian and S. V. Vladimirov, Phys. Rev. E **67**, 066404 (2003).
[17] A. A. Samarian, S. V. Vladimirov, and B. W. James, Phys. Plasmas **12**, 022103 (2005).
[18] N. C. Adhikary, H. Bailung, A. R. Pal, J. Chutia, and Y. Nakamura, Phys. Plasmas **14**, 103705 (2007).
[19] Y. C. Hong, J. H. Kim, C. U. Bang, and H. S. Uhm, Phys. Plasmas **12**, 114501 (2005).
[20] L. Wang, L. Cui, X. D. Zhu, and X. H. Wen, Phys. Plasmas **14**, 123501 (2007).
[21] J. D. Long, S. Xu, S. Y. Huang, P. P. Rutkevych, M. Xu, and C. H. Diong, IEEE Trans. Plasma Sci. **33**, 240 (2005).
[22] K. Koga, S. Iwashita, and M. Shiratani, J. Phys. D **40**, 2267 (2007).
[23] M. S. Bell, K. B. K. Teo, and W. I. Milne, J. Phys. D **40**, 2285 (2007).
[24] K. Ostrikov, Rev. Mod. Phys. **77**, 489 (2005).
[25] K. Ostrikov, IEEE Trans. Plasma Sci. **35**, 127 (2007).
[26] I. Levchenko and K. Ostrikov, J. Phys. D **40**, 2308 (2007).
[27] P. P. Rutkevych, K. Ostrikov, and S. Xu, Phys. Plasmas **14**, 043502 (2007).
[28] S. J. Choi and M. J. Kushner, Appl. Phys. Lett. **62**, 2197 (1993).
[29] M. S. Barnes, J. H. Keller, J. C. Forster, J. A. O'Neill, and D. K. Coultas, Phys. Rev. Lett. **68**, 313 (1992).
[30] C. Zafiu, A. Melzer, and A. Piel, Phys. Rev. E **63**, 066403 (2001).
[31] M. Salimullah, I. Sandberg, and P. K. Shukla, Phys. Rev. E **68**, 027403 (2003).
[32] M. Y. Yu, H. Saleem, and H. Luo, Phys. Fluids B **4**, 3427 (1992).
[33] T. Nitter, Plasma Sources Sci. Technol. **5**, 93 (1996).
[34] J. X. Ma and M. Y. Yu, Phys. Plasmas **2**, 1343 (1995).
[35] J. X. Ma, J.-Y. Liu, and M. Y. Yu, Phys. Rev. E **55**, 4627 (1997).
[36] V. N. Tsytovich, S. V. Vladimirov, and S. Benkadda, Phys. Plasmas **6**, 2972 (1999).

[37]G. C. Das and P. Kalita, J. Phys. D **37**, 702 (2004).
[38]D. P. Resendes, G. Sorasio, and P. K. Shukla, Phys. Plasmas **9**, 2988 (2002).
[39]D. P. Resendes, G. Sorasio, and P. K. Shukla, Phys. Scr. **98**, 87 (2002).
[40]J.-Y. Liu, Z.-X. Wang, X. Wang, Q. Zhang, X. Zou, and Y. Zhang, Phys. Plasmas **10**, 3507 (2003).
[41]M. Davoudabadi and F. Mashayek, Phys. Plasmas **12**, 073505 (2005).
[42]M. Davoudabadi, B. Rovagnati, and F. Mashayek, IEEE Trans. Plasma Sci. **34**, 142 (2006).
[43]B. P. Pandey, A. Samarian, and S. V. Vladimirov, Phys. Plasmas **14**, 093703 (2007).
[44]G. Foroutan, H. Mehdipour, and H. Zahed, Phys. Plasmas **16**, 103703 (2009).
[45]I. Levchenko, K. Ostrikov, M. Keidar, and S. Xu, J. Appl. Phys. **98**, 064304 (2005).
[46]S. Xu, K. Ostrikov, J. D. Long, and S. Y. Huang, Vacuum **80**, 621 (2006).
[47]I. Levchenko, K. Ostrikov, M. Keidar, and S. V. Vladimirov, Phys. Plasmas **14**, 113504 (2007).
[48]K. Ostrikov and A. B. Murphy, J. Phys. D **40**, 2223 (2007).
[49]I. Levchenko, K. Ostrikov, J. D. Long, and S. Xu, Appl. Phys. Lett. **91**, 113115 (2007).
[50]I. Levchenko, K. Ostrikov, A. E. Rider, E. Tam, S. V. Vladimirov, and S. Xu, Phys. Plasmas **14**, 063502 (2007).
[51]I. Levchenko and K. Ostrikov, Nanotechnology **19**, 335703 (2008).
[52]I. Levchenko, K. Ostrikov, K. Diwan, K. Winkler, and D. Moriotti, Appl. Phys. Lett. **93**, 183102 (2008).
[53]I. Levchenko, K. Ostrikov, D. Moriotti, and A. B. Murphy, J. Appl. Phys. **104**, 073308 (2008).
[54]K. Ostrikov, *Plasma Nanoscience: Basic Concepts and Applications of Deterministic Nanofabrication* (Wiley, Weinheim, 2008).
[55]P. K. Shukla and A. A. Mamun, *Introduction to Dusty Plasma Physics* (IOP, Bristol, 2002).
[56]P. P. Rutkevych, K. Ostrikov, and S. Xu, Phys. Plasmas **12**, 103507 (2005).
[57]P. P. Rutkevych, K. Ostrikov, S. Xu, and S. V. Vladimirov, J. Appl. Phys. **96**, 4421 (2004).
[58]J.-G. Li, M. Ikeda, R. Ye, Y. Moriyoshi, and T. Ishigaki, J. Phys. D: Appl. Phys. **40**, 2348 (2007).
[59]V. E. Fortov, O. S. Vaulina, O. F. Petrov, V. I. Molotkov, A. M. Lipaev, G. E. Morfill, H. Thomas, S. A. Khrapak, Yu. P. Semenov, and A. I. Ivanov, Plasma Phys. Controlled Fusion **46**, B359 (2004).
[60]V. E. Fortov, A. P. Nefedov, V. I. Molotkov, M. Y. Poustylnik, and V. M. Torchinsky, Phys. Rev. Lett. **87**, 205002 (2001).
[61]Q.- Z. Luo and N. D´Angelo, J. Phys. D **33**, 2754 (2000).
[62]U. Mohideen, H. U. Rahman, M. A. Smith, M. Rosenberg, and D. A. Mendis, Phys. Rev. Lett. **81**, 349 (1998).
[63]M. A. Smith, J. Goodrich, H. U. Rahman, and U. Mohideen, IEEE Trans. Plasma Sci. **29**, 216 (2001).